

RAPID COMMUNICATION

Synthesis and Structure of Cobalt (II) Oxide Halides— $\text{Sr}_2\text{CoO}_2\text{X}_2$ ($X=\text{Cl}, \text{Br}$)

Christopher S. Knee and Mark T. Weller¹

Department of Chemistry, University of Southampton, Southampton SO17 1BJ, United Kingdom

Received March 4, 2002; in revised form June 6, 2002; accepted June 17, 2002

The first layered cobalt (II) oxide halides, $\text{Sr}_2\text{CoO}_2\text{Cl}_2$ and $\text{Sr}_2\text{CoO}_2\text{Br}_2$, have been synthesized and their structures determined from Rietveld refinement of powder X-ray data. The materials are structural analogues of the K_2NiF_4 cuprate phase $\text{Sr}_2\text{CuO}_2\text{Cl}_2$, crystallizing in space group $I4/mmm$. The compounds contain CoO_2 square planes separated by SrX layers ($X=\text{Cl}, \text{Br}$). The bromide material displays the expected increase in cell dimensions, i.e., for $\text{Sr}_2\text{CoO}_2\text{Cl}_2$, $a = 4.06251(5) \text{ \AA}$, $c = 15.1251(3) \text{ \AA}$ and for $\text{Sr}_2\text{CoO}_2\text{Br}_2$, $a = 4.08891(7) \text{ \AA}$, $c = 16.4077(4) \text{ \AA}$. © 2002 Elsevier Science (USA)

Key Words: oxyhalide; K_2NiF_4 -type structure; anion ordered; cobalt (II); powder X-ray diffraction.

INTRODUCTION

In recent years, the remarkable properties of superconductivity and magnetoresistance displayed by first row transition metal oxides has produced considerable activity in terms of the synthesis of new complex oxides (1). The search for new layered materials has also led to the development of mixed anion systems, such as oxide carbonates (2), oxide borates (3) and oxide halides (4). For the latter class of compounds this has resulted in a wide range of complex copper oxide halide superconductors, such as $(\text{Ca}, \text{Na})_2\text{CuO}_2\text{Br}_2$ with a $T_c = 24 \text{ K}$ (5), developed from the oxychloride $\text{Sr}_2\text{CuO}_2\text{Cl}_2$ first reported by Grande and Müller-Buschbaum (6). $\text{Sr}_2\text{CuO}_2\text{Cl}_2$ has since received significant interest as an ideal system for studying the two-dimensional antiferromagnetic (AF) interactions that occur within the CuO_2 planes of an undoped superconductor (7).

Other transition metal oxyhalide phases include the iron and cobalt Ruddlesden–Popper-related phases described

by the general formulas, $A_{n+1}M_n\text{O}_{3n}X$, $n = 1$ e.g., $\text{Ca}_2\text{FeO}_3\text{Cl}$ (4) and $A_{n+1}M_n\text{O}_{3n-1}X_2$, $n = 2, 3$ e.g., the $n = 2$ phase $\text{Sr}_3\text{Co}_2\text{O}_5\text{Cl}_2$ (8). Recently we have expanded this oxide halide family, synthesizing the manganese phases, $\text{Sr}_2\text{MnO}_3\text{Cl}$ and $\text{Sr}_4\text{Mn}_3\text{O}_{8-y}\text{Cl}_2$ (9). The single-layer $n = 1$ materials are formally the end member of Ruddlesden–Popper family $\text{Sr}_{n+1}M_n(\text{O}, \text{Cl})_{3n+1}$ where either one or two halides replace oxygen in the terminal position. Within this system variation of the oxide-to-halide ratio permits control of the transition metal oxidation state from +3 e.g., $\text{Sr}_2\text{MnO}_3\text{Cl}$ to +2 e.g., $\text{Sr}_2\text{CuO}_2\text{Cl}_2$. In this communication we report the synthesis and structure of two new cobalt (II) oxyhalide materials, $\text{Sr}_2\text{CoO}_2\text{Cl}_2$ and $\text{Sr}_2\text{CoO}_2\text{Br}_2$, that are direct structural analogues of $\text{Sr}_2\text{CuO}_2\text{Cl}_2$. The materials contain CoO_2 sheets that are separated by nonmagnetic SrX_2 layers.

EXPERIMENTAL

Polycrystalline samples of $\text{Sr}_2\text{CoO}_2\text{X}_2$ ($X=\text{Cl}$ and Br) were synthesised by reaction of stoichiometric amounts of SrO (from SrCO_3 at 1050°C for 4 days), SrX_2 (Aldrich 99.99%) and CoO (Aldrich 99.99%) in silica ampoules sealed under vacuum. The reagents were ground in a dry box ($<1 \text{ ppm O}_2/\text{H}_2\text{O}$), transferred to the reaction vessel and fired for 16 h at 850°C for $\text{Sr}_2\text{CoO}_2\text{Cl}_2$ and 625°C for $\text{Sr}_2\text{CoO}_2\text{Br}_2$. The products were pale purple powders, $\text{Sr}_2\text{CoO}_2\text{Cl}_2$ being insensitive to atmospheric conditions whilst $\text{Sr}_2\text{CoO}_2\text{Br}_2$ was found to decompose on prolonged exposure to moisture in the air.

Sample purity was assessed from powder X-ray data collected using a Bruker D8 diffractometer ($\text{CuK}\alpha_1$) operating with a position sensitive detector. For both materials all major peaks could be accounted for on the basis of a tetragonal $I4/mmm$ unit cell. The only impurity apparent for the $\text{Sr}_2\text{CoO}_2\text{Cl}_2$ sample was a trace level of

¹To whom correspondence should be addressed. Fax: +00-44-2380-593592. E-mail: mtw@soton.ac.uk.



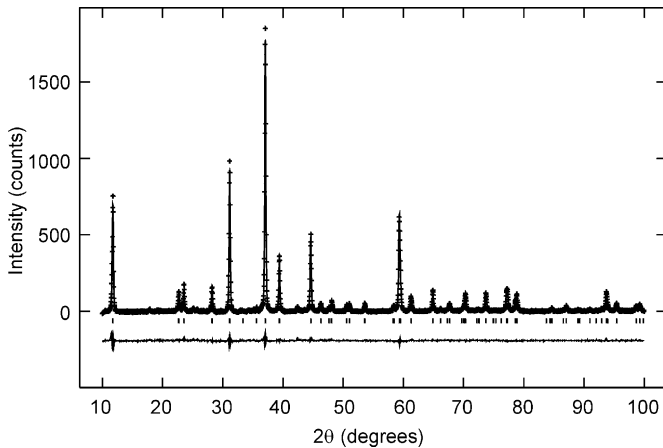


FIG. 1. Fit obtained to the powder X-ray diffraction data from $\text{Sr}_2\text{CoO}_2\text{Cl}_2$. Crosses are observed data, upper continuous line the fitted profile, lower line the difference and tick marks show the reflection positions.

CoO. The $\text{Sr}_2\text{CoO}_2\text{Br}_2$ scan revealed a slightly greater level of CoO and additional weak intensity (estimated at $<5\%$ from the most intense line) of an unidentified impurity. Further high quality powder X-ray diffraction data were collected in the 2θ range $10\text{--}100^\circ$ step size 0.017° over a period of 10 h on both materials (the Br sample mounted under a layer of Mylar) and a structural model derived from $\text{Sr}_2\text{CuO}_2\text{Cl}_2$ refined using Rietveld profile analysis (10). Refinements were completed to convergence with the variation of positional and thermal parameters of all atoms except for the oxygen ions whose B factors were fixed at 2.0 \AA^2 . The $\text{Sr}_2\text{CoO}_2\text{Cl}_2$ analysis revealed discrepancies in intensity on certain $(0,0,l)$ reflections, which were corrected satisfactorily by modelling the effects of preferred orientation. As a final step CoO was introduced into the

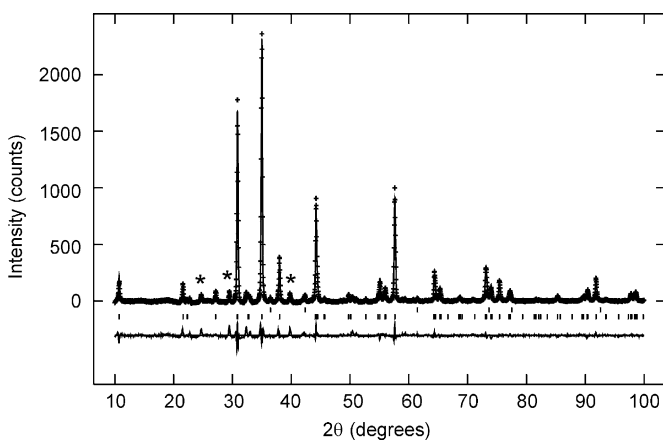


FIG. 2. Fit obtained to the powder X-ray diffraction data from $\text{Sr}_2\text{CoO}_2\text{Br}_2$. Crosses are observed data, upper continuous line the fitted profile, lower line the difference. Upper (lower) tick marks show the reflection positions for $\text{Sr}_2\text{CoO}_2\text{Br}_2$ (CoO). * Indicates the positions of reflections from an unidentified impurity.

TABLE 1
Structural and Fit Parameters for the $\text{Sr}_2\text{CoO}_2\text{X}_2$ Materials

Atom	Site	$\text{Sr}_2\text{CoO}_2\text{Cl}_2$		$\text{Sr}_2\text{CoO}_2\text{Br}_2$	
		z	$B_{\text{iso}} (\text{\AA}^2)$	z	$B_{\text{iso}} (\text{\AA}^2)$
Sr	$(0,0,z) 4e$	0.3914(1)	1.59(2)	0.3994(1)	1.73(6)
Co	$(0,0,0) 2a$	—	1.53(6)	—	0.46(10)
O	$(0, \frac{1}{2}, 0) 4c$	—	2.00	—	2.00
X	$(0,0,z) 4e$	0.1815(1)	1.76(6)	0.1772(1)	1.82(8)
a (\AA)		4.06251(5)		4.08891(7)	
c (\AA)		15.1251(3)		16.4077(4)	
χ^2		3.51		5.05	
R_{wp} (%)		1.30		2.30	
R_{p} (%)		0.85		1.42	

Note. Space group $I4/mmm$ (esds are given in parentheses).

$\text{Sr}_2\text{CoO}_2\text{Br}_2$ analysis (weight fraction = 3%). The fit to the profiles achieved for $\text{Sr}_2\text{CoO}_2\text{Cl}_2$ and $\text{Sr}_2\text{CoO}_2\text{Br}_2$ are shown in Figs. 1 and 2, and the coordinate descriptions obtained, together with profile fit factors, are summarized in Table 1.

The magnetic susceptibility of $\text{Sr}_2\text{CoO}_2\text{Cl}_2$ over the temperature range $320\text{--}10 \text{ K}$ was determined using a Cryogenics S600 SQUID magnetometer. Data were collected after cooling the sample in the absence of an applied field (ZFC) and after cooling in the measuring field (FC) of 100 G.

RESULTS AND DISCUSSION

The structure of the $\text{Sr}_2\text{CoO}_2\text{X}_2$ materials is shown in Fig. 3. The cobalt coordination may be viewed as square planar with respect to oxygen or as highly elongated octahedra if the Co–X interactions are included. As for other K_2NiF_4 materials, such as Sr_2MnO_4 , strontium is formally in nine-fold coordination. However, the increased size of the halide in comparison to the oxide ion results in a more distorted environment, e.g., for $\text{Sr}_2\text{CoO}_2\text{Cl}_2$ $4 \times \text{Sr}\text{--O}$ bonds at 2.6 \AA , $4 \times \text{Sr}\text{--Cl}$ bonds at 3.1 \AA and one longer Sr–Cl interaction at 3.17 \AA (Table 2). The larger halide causes the Sr ion to move towards the CoO_2 plane resulting in highly puckered SrX rocksalt layers.

The refined cell parameters (Table 1) show the expected increase for the bromide phase, with a small 0.03 \AA increase in a and a much more significant enlargement of 1.3 \AA along c . These trends are reflected in the cobalt coordination. The in-plane Co–O bond increases from 2.031 \AA in $\text{Sr}_2\text{CoO}_2\text{Cl}_2$ to 2.044 \AA in $\text{Sr}_2\text{CoO}_2\text{Br}_2$ and the Co–X apical interaction from 2.75 to 2.91 \AA in line with the ionic radii of Shannon, i.e. $\text{Cl}^- = 1.81 \text{ \AA}$ and $\text{Br}^- = 1.96 \text{ \AA}$ (11). The main structural factor responsible for the large

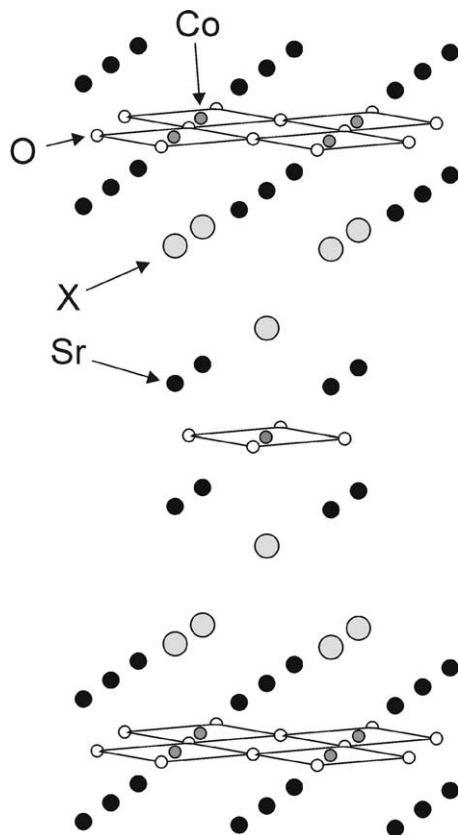


FIG. 3. The structure of the $\text{Sr}_2\text{CoO}_2\text{X}_2$ phases showing the network of cobalt–oxygen square planes of stoichiometry CoO_2 .

increase in the c -parameter of $\text{Sr}_2\text{CoO}_2\text{Br}_2$ is the greater halide repulsion between inter-layer bromide ions that increases the vertical separation of neighboring Br^- ions to 2.41 Å from the 2.07 Å in $\text{Sr}_2\text{CoO}_2\text{Cl}_2$. This effect is also shown clearly in the single Sr–X halide bond (Table 2), which increases from 3.175 to 3.644 Å whilst the Sr–O distance remains constant at approximately 2.6 Å.

The coordination of cobalt to oxygen within the $\text{Sr}_2\text{CoO}_2\text{X}_2$ materials differs from that of the previously reported cobalt oxychlorides (8). In the phase $\text{Sr}_2\text{CoO}_3\text{Cl}$, cobalt (III) is formally coordinated to oxygen in a square

TABLE 2
Selected Interatomic Distances Obtained
for $\text{Sr}_2\text{CoO}_2\text{X}_2$ Materials

Distance (Å)	$\text{Sr}_2\text{CoO}_2\text{Cl}_2$	$\text{Sr}_2\text{CoO}_2\text{Br}_2$
Co–O × 4	2.03126(2)	2.04445(4)
Co–X × 2	2.745(2)	2.908(2)
Sr–O × 4	2.6124(7)	2.628(1)
Sr–X × 4	3.0768(8)	3.153(1)
Sr–X × 1	3.175(2)	3.644(2)

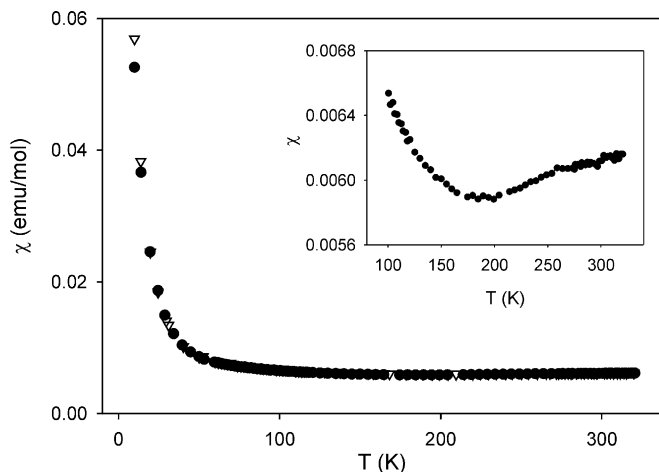


FIG. 4. Magnetic susceptibility vs temperature for $\text{Sr}_2\text{CoO}_2\text{Cl}_2$. Closed circles and open triangles are ZFC and FC data, respectively. The inset shows the ZFC data in the range 320–100 K.

pyramidal arrangement with a single interaction to chloride. The observed bond lengths also reflect the higher cobalt oxidation state, with in-plane bonds of 1.978 Å and an apical Co–O distance of 1.895 Å. Interestingly, the Co–Cl bond in the Co(III) compound at 3.116 Å is significantly longer than that determined for $\text{Sr}_2\text{CoO}_2\text{Cl}_2$. A comparison of the cobalt and copper environments in the $\text{Sr}_2\text{CoO}_2\text{X}_2$ and $\text{Sr}_2\text{CuO}_2\text{X}_2$ (6) materials reveal a more distorted coordination for the cuprates, consistent with the Jahn–Teller effect for Cu^{2+} . Considering the chloride phases, the Cu–O bond is 1.986 Å and the Cu–Cl distance is 2.859 Å compared with a Co–O bond of 2.031 Å and Co–Cl interaction of 2.745 Å.

Figure 4 plots the magnetic susceptibility of $\text{Sr}_2\text{CoO}_2\text{Cl}_2$ over the temperature range 320–10 K. The susceptibility shows a small drop down to approximately 200 K (see inset) before displaying a paramagnetic increase on cooling below 50 K. The magnetic behavior is similar to that previously reported for polycrystalline samples of the closely related K_2NiF_4 -type phase $\text{La}_2\text{CoO}_{4+\delta}$ with $\delta \approx 0.1$ (12) over the same temperature range and suggests the material orders antiferromagnetically at $T > 320$ K. However, the effect is small and the presence of CoO impurity means that definitive conclusions will require further experiments. For example, neutron diffraction has been used to confirm the presence of successive AF phase transitions in single crystals of stoichiometric La_2CoO_4 (13).

In summary, two new Co(II) oxide halides isostructural with the antiferromagnetic cuprate phase $\text{Sr}_2\text{CuO}_2\text{Cl}_2$ have been synthesized and their structures determined from Rietveld refinement of powder X-ray diffraction data. Further studies into the magnetic properties these materials display are planned.

ACKNOWLEDGMENT

We thank the EPSRC for support for this work under Grant GR/M21836.

REFERENCES

1. M. T. Weller and C. S. Knee, *J. Mat. Chem.* **11**, 701 (2001).
2. K. Yamaura, Q. Huang, J. W. Lynn, R. W. Erwin, and R. J. Cava, *J. Solid State Chem.* **152**, 374 (2000).
3. D. Pelloquin, M. Hervieu, C. Michel, N. Nguyen, and B. Raveau, *J. Solid State Chem.* **34**, 395 (1997).
4. J. F. Ackerman, *J. Solid State Chem.* **92**, 496 (1991).
5. S. Adachi, T. Tatsuki, T. Tamura, and K. Tanabe, *Chem. Mater.* **10**, 2860 (1998).
6. B. Grande and Hk. Müller-Buschbaum, *Z. Anorg. Allg. Chem.* **417**, 68 (1975).
7. D. Vankin, L. L. Miller, J. L. Zarestky, and D. C. Johnston, *Physica C* **274**, 331 (1997).
8. S. M. Loureiro, C. Felser, Q. Huang, and R. J. Cava, *Chem. Mater.* **12**, 3181 (2000).
9. C. S. Knee and M. T. Weller, *Chem. Commun.* **3**, 256 (2002).
10. A. C. Larson and R. B. von Dreele, "Generalised Structure Analysis System," Los Alamos National Laboratory, Los Almos, 1994.
11. R. D. Shannon, *Acta Crystallogr. A* **32**, 751 (1976).
12. R. A. Mohan Ram, P. Ganguly, and C. N. R. Rao, *Mater. Res. Bull.* **23**, 501 (1988).
13. Y. Yamada, M. Matsuda, Y. Endoh, B. Keimer, R. J. Birgeneau, S. Onodera, J. Mizusaki, T. Matsuura, and G. Shirane, *Phys. Rev. B* **39**, 2336 (1989).